Supporting Information

Long-term cropping rotation with soybean enhances soil health as evidenced by improved nutrient cycles through keystone phylotypes interaction

Xiaowei Huang[1,2], Jing Yuan[3], Yuxuan Chen[1,2], Xueling Yang[1,2], Wencheng Lu[4], Surong Ding[5], Yu Jiang[4], Xuechao Zhou[5], Gang Mi[4], Jianming Xu[1,2], Yan He[1,2*]

1 Zhejiang Provincial Key Laboratory of Agricultural Resources and Environment, Institute of Soil and Water Resources and Environmental Science, College of Environmental and Resource Sciences, Zhejiang University, Hangzhou 310058, China

2 Key Laboratory of Environment Remediation and Ecological Health, Ministry of Education, Hangzhou 310058, China

3 Microbiome Network and Department of Agricultural Biology, Colorado State University, Fort Collins, 80524, USA.

4 Heihe Branch of Heilongjiang Academy of Agricultural Sciences, Heihe 164300, China

5 Chifeng Agricultural and Animal Husbandry Research Institute, Chifeng 024031, China

** Corresponding author: Yan He; E-mail: yhe2006@zju.edu.cn; Tel.: +86-571-8898-2065; Fax: +86-571-8898-2065*

S1 Physicochemical parameters analyses

Physicochemical parameters were measured according to previously described (Feng et al., 2019; Huang et al., 2021; Xu et al., 2015). In brief, soil pH was determined by a pH meter (S975 SevenExcellence, MettlerToledo, Switzerland) in a suspension of a 1:2.5 soil/water ratio (w/v). DOC and DON were extracted with Milli-Q water and measured with ion chromatography (Dionex ICS-2000, United States). TC and TN in the freeze-dried soil samples were measured with an element analyzer (Elementar Vario EL cube, Germany). Levels of NO_3^--N and NH_4^+-N in the soil samples were measured using a continuous flow analyzer (TRAACS 2000, Bran and Luebbe, Norderstedt, Germany) after extraction with 1 mol·L^{-1} KCl (1:5, w/v). The concentration of Fe^{2+} and AFe (with hydroxylamine hydrochloride for reduing Fe^{3+} to Fe^{2+}, then total of in Fe^{2+} solution repsented total available iron) was measured using the 1,10-phenanthroline colorimetric method at

510 nm on a UV–Vis spectrophotometer (Thermofisher, USA), and the concertration of AFe minus Fe^{2+} is the concertration of Fe^{3+}. The quantification of AP was using the molybdenum blue method at 880 nm on a UV–Vis spectrophotometer (Thermofisher, USA).

S2 Herbicide residue extraction and quantification of soil samples

Herbicide extraction The 2g soil sample was weighed into the 50ml centrifuge tube. Further, 10ml ultra-pure water was added to soak for 10 min, and then 10mL HPLC acetonitrile (Merk, Germany) was added to vortex for 2min. After that, 4g $MgSO_4$ and 1g NaCl was applied to stimulate partition. After 4000rpm centrifugation for 5min, the supernatant was transferred to another centrifuge tube containing 900mg $MgSO_4$ and 100mg C18, then the tube was shook by hand for 15 seconds and vibrated for 2 mins Finally, the supernatant filter membrane was analyzed in the injection bottle after 4000rpm centrifugation and 5min.

Instrumental quantification An ACQUITY I-class ultra-performance liquid chromatograph coupled with a TQ-XS tandem mass spectrometer (Waters, Milford, MA) was used for quantification of herbicides. The column used for test: ACQUITY BEH C18 column (2.1 mm × 50 mm, 1.7μm). The temperature of column was set as 40℃. Mobile phase (A) contained water/0.1% formic acid, mobile phase (B) was HPLC acetonitrile. The gradient program was as follows: 0-1.5min, 10-40% B; 1.5-4.0min 40-50% B; 4.0-6.0min 50-100% B; 6.0-7.5min 100% B; 7.5-10.0min 100-10% B. Flow rate was 0.2 mL/min and injection volume was 5 uL.

The optimal parameters of mass spectrometer were employed as follows: Desolvation gasflow, 800 L/Hr; cone airflow, 150L/Hr; collision gasflow, 0.15 mL/min. Multiple reaction monitoring (MRM) mode was applied for analysis.

S3 The primers and analysis for the amplification of 16S rRNA and ITS

The primers 515F (5′-GTGCCAGCMGCCGCGGTAA -3′) and 806R (5′-CCGTCAATTCMTTTRAGTTT′) amplifying the V4-V5 region of the bacterial 16S rRNA gene and the primers ITS3-F (5′-GCATCGATGAAGAACGCAGC-3′) and ITS4-R (5′-TCCTCCGCTTATTGATATGC′) amplifying the ITS2 region of the fungal ITS gene were used for PCR amplification. DNA amplicon sequences were analyzed on the Illumina Nova6000 platform from Guangdong Magigene Biotechnology Co. Ltd., Guangzhou, China.

S4 Ecological multifunctionality and biodiversity

We averaged the normalized scores of all individual functional genes and obtain an averaging

multifunctionality index. For the multithreshold multifunctionality approach, the critical threshold (>10%, 25%, 50%, 75%, 90%) was set simultaneously in this study (Delgado-Baquerizo et al., 2020), to assess the relationships of soil biodiversity with the number of soil ecological functions.

The richness of bacteria, fungi, and the bacteria-fungi community were highly correlated with Shannon index in all cases (Fig. S2), suggesting whichever is chosen will not affect the results. The calculation of the biodiversity of soil organisms was similar to the averaging multifunctionality index: we averaged the normalized scores (min-max normalization) of the richness of the microbial community to represented biodiversity.

S5 The construction of Co-occurrence network and further analyses

First, in this study, to reduce potential spurious correlations from the extremely rare taxa, we focused on the domain phylotypes which were ubiquitous (>35% for bacteria and fungi of all samples) (Delgado-Baquerizo et al., 2020; Jiao et al., 2022). After filtering, the Spearman correlation networks were conducted to identify ecological clusters of strongly associated soil phylotypes. Then we used R package *neten* (Zhao et al., 2021) and R package *RMThreshold* (Luo et al., 2006) with correlation cut-off of $p < 0.001$ (p values were adjusted by false-discovery-rate method), and obtain denoised co-occurrence networks. The visualization of networks was executed with the interactive platform Gephi_0.9.2 and R package *igraph*, while the ecological cluster was identified using the Gephi_0.9.2 (Fan et al., 2020). The biodiversity (normalized richness index) of soil phylotypes within each ecological cluster was calculated subsequently as the method described in SI S4. The topological parameters of the extracted subnetworks by preserving the phylotypes and their correlations from networks of individual soil samples were calculated (Jiao et al., 2022), for exploring the potential effects of the complexity of networks on soil multifunctionality,

The participation coefficient *Pi* measures how 'well-distributed' the links of node are among different clusters (Guimera and Amaral, 2005). The calculation of *Pi* was processed according to previous study (Cumbo et al., 2014):

$$P_i = 1 - \left(\frac{k_i^{in}}{k_i} \right)^2$$

where $k_i^{in}$is the the number of links of node *i* with nodes in its own cluster, k_i is the total degree of node *i*. After identifying connectors in clusters (*Pi* > 0.62, Fig. S10A), to excavate the interactions

among keystone clusters, we further extracted keystone clusters 1, 2 and 4 from network (processing in R package *igraph*), and recalculating the *Pi* values of connectors (occuring in keystone clusters), then we found these connectors in cluster 1, 2 and 4 still conform to $Pi > 0.62$, indicating that these connectors are only responsible for connecting these key clusters (Fig. S10C).

S6 Linking the biodiversity and multifunctionality

The least significant difference (LSD) method was employed to compare and evaluate the differences between the different cropping patterns. The *Tax4Fun2* R package was used to predict bacterial community potential based on the KEGG pathway and functional redundancy indices. Ordinary least squares linear regressions (OLS) were conducted to link soil microbial biodiversity to multifunctionality. We conducted Spearman correlations to analyze the associations between the biodiversity of phylotypes and functions. We used R packages *rfPermute* and *A3* (Fortmann-Roe, 2015) to conduct a classification random forest analysis of the major soil microbial groups in driving soil ecological multifunctionality.

S7 Bacterial whole-genomes downloading and annotation

15 bacterial complete genomes were downloaded from GeneBank (ftp://ftp.ncbi.nlm.nih.gov/genomes/genbank/bacteria/, Table S8). Gene predictions were performed using Prodigal v2.6.3 with default parameters. The genes involved in C cycles and the degradation of herbicides were annotated by eggNOG-mapper 2.1.9 (--database bact -m diamond --sensmode ultra-sensitive –evalue 10^{-5}) with eggNOG 5.0 (KEGG) (Huerta-Cepas et al., 2019); genes involved in N, P and S cycles were annotated with Diamond v2.0.15 (--ultra-sensitive –evalue 10^{-5}) (Buchfink et al., 2021) with NCycDB (Tu et al., 2019), PCycDB (Zeng et al., 2022) and SCycDB (Yu et al., 2021), respectively.

S8 Soil quality indices

We used soil parameters of rotation for subsequent standardization. The areas on a radar chart of a combination of multiple soil indices included abiotic parameters (DOC, DON, NH_4^+-N, Fe^{2+}, Fe^{3+}, AFe, AP, TC, TN, C/N and 23 kinds of herbicides residue) and biotic parameters (63 detected and quantified functional genes and multiversity of key-stone phylotypes/connectors) were calculated as the standardized parameters. Considering the potential negative effects of herbicides residue on soil functions in our study (Fig. 4) and the ecological sense of C/N ratio (Sun et al., 2022), we inversed these variables for further SQI area calculations (-1×value of total herbicide residues

or C/N ratio), and we also used rotation soil ($SQI_{rotation}$) to obtain the relative SQI (($SQI_i/SQI_{rotation}$)-1, where SQI_i is the SQI area value of different cropping strategies, $SQI_{rotation}$ is the values of SQI area in rotation soil). All parameters were normalized with min-max normalization before assessment.

Table S1 Soil herbicide residues extracted and quantified in this study (classified by chemical properties)

Chemical classification	Herbicides
Sulfonylureas	Tribenuron Methyl
	Bensulfuron-methyl
	Rimsulfuron
	Thifensulfuron-methyl
	Nicosulfuron
	Halosulfuron-methyl
Amides	Acetochlor
	Alachlor
Triazine	Atrazine
	Simazine
	Simetryn
	Metribuzin
Aryloxyphenoxypropionate	Quizalofop-P
	Fenoxaprop-P
Cyclic imine	Flumioxazin
Heterocycles	Clomazone
	Bentazone
Phenoxy acid	(4-chloro-2-methylphenoxy)Acetic acid
Substituted urea	Chlorotoluron
	Isoproturon
Diphenyl ether	Fomesafen
Imidazolinone	5,6-bis(4-methoxyphenyl)-2,3-diphenylthieno[3,2-b]Furan
Benzoylcyclohexanediones	Mesotrione

Table S2 The information of 71 functional genes quantifying on Wafergen Smart Chip Real-Time qPCR platform

Gene	Classfication	Ecoding protein	Function
abf A	C degradation	α-L-arabinofuranosidase	Hemicellulose hydrolysis
amy A	C degradation	α-amylase	Starch hydrolysis
amy X	C degradation	pullulanase	Starch hydrolysis
apu	C degradation	amylopullulanase	Starch hydrolysis
cdh	C degradation	cellobiose dehydrogenase	Cellulose hydrolysis
cex	C degradation	exoglucanase	Cellulose hydrolysis

chi A	C degradation	endochitinase	Chitin hydrolysis
exo-chi	C degradation	exochitinase	Chitin hydrolysis
glx	C degradation	glyoxal oxidase	Lignin hydrolysis
iso-plu	C degradation	Isopullulanase	Starch hydrolysis
lig	C degradation	lignin peroxidase	Lignin hydrolysis
man B	C degradation	β- mannanase	Hemicellulose hydrolysis
mnp	C degradation	manganese peroxidase	Lignin hydrolysis
naglu	C degradation	α-N-acetylglucosaminidase	Cellulose hydrolysis
pgu	C degradation	pectinase/polygalacturonase	Pectin hydrolysis
pox	C degradation	phenol oxidase	Lignin hydrolysis
gam	C degradation	glucoamylase	Starch hydrolysis
xyl A	C degradation	xylose isomerase	Hemicellulose hydrolysis
acc A	C fixation	acetyl-CoA carboxylase carboxyltransferase α subunit	C fixation
acl B	C fixation	ATP-citrate lyase β subunit	C fixation
acs A	C fixation	acetyl-coenzyme A synthetase	C fixation
acs B	C fixation	acetyl-CoA synthase complex β subunit	C fixation
acs E	C fixation	5-methyltetrahydrofolate corrinoid methyltransferase	C fixation
cda R	C fixation	carbohydrate diacid regulon transcriptional regulator	C fixation
frd A	C fixation	fumarate reductase flavoprotein subunit	C fixation
kor A	C fixation	2-oxoglutarate ferredoxin oxidoreductase α subunit	C fixation
mct	C fixation	mesaconyl-CoA C1-C4 CoA transferase	C fixation
mcr A	C fixation	methyl-coenzyme M reductase α subunit	C fixation
pcc A	C fixation	acetyl/propionyl-CoA carboxylase alpha	C fixation
rbc L	C fixation	ribulose-bisphosphate carboxylase large chain	C fixation
smt A	C fixation	succinyl-CoA:(S)- malate CoA transferase	C fixation
mmo X	Methane metabolism	methane monooxygenase component A alpha chain	Methane oxidation
mxa F	Methane metabolism	methanol dehydrogenase (cytochromec) subunit 1	Methane production
pgg-mdh	Methane metabolism	methanol/ethanol family PQQ-dependent dehydrogenase	Methane production
pmo A	Methane metabolism	methane/ammonia monooxygenase subunit A	Methane oxidation
amo A1	N Cycling	ammonia monooxygenase α subunit (Archaea)	Aerobic ammoxidation

amo A2	N Cycling	ammonia monooxygenase α subunit (Bacteria)	Aerobic ammoxidation
amo B	N Cycling	ammonia monooxygenase β subunit	Aerobic ammoxidation
gdh A	N Cycling	glutamate dehydrogenase	Organic N mineralization
hao	N Cycling	hydroxylamine oxidoreductase	Nitrification
hzo	N Cycling	hydrazine oxidase	Anaerobic ammonium oxidation
hzs A	N Cycling	hydrazine synthase α subunit	Anaerobic ammonium oxidation
hzs B	N Cycling	hydrazine synthase β subunit	Anaerobic ammonium oxidation
nap A	N Cycling	periplasmic nitrate reductase	Denitrification
nar G	N Cycling	nitrate reductase α chain	Denitrification
nas A	N Cycling	assimilatory nitrate reductase catalytic subunit	Denitrification
nif H	N Cycling	nitrogenase iron protein	N fixation
nir K1	N Cycling	nitrite reductase (NO-forming)	Denitrification
nir K2	N Cycling	nitrite reductase (NO-forming)	Denitrification
nir K3	N Cycling	nitrite reductase (NO-forming)	Denitrification
nir S1	N Cycling	nitrite reductase (NO-forming)	Denitrification
nir S2	N Cycling	nitrite reductase (NO-forming)	Denitrification
nir S3	N Cycling	nitrite reductase (NO-forming)	Denitrification
nos Z1	N Cycling	nitrous-oxide reductase	Denitrification
nos Z2	N Cycling	nitrous-oxide reductase	Denitrification
nxr A	N Cycling	nitrite oxidoreductase α subunit	Nitrification
ure C	N Cycling	urease	Organic N mineralization
bpp	P Cycling	β-propeller phytase	Organic P mineralization
cphy	P Cycling	ruminal cysteine phytase	Organic P mineralization
gcd	P Cycling	quinoprotein glucose dehydrogenase	Inorganic P solubilization
phn K	P Cycling	phosphonate transport system ATP-binding protein	Organic P mineralization
pho D	P Cycling	alkaline phosphatase D	Organic P mineralization
pho X	P Cycling	alkaline phosphatase/Pho regulon	Organic P mineralization
ppk	P Cycling	polyphosphate kinase	Inorganic P biosynthesis
ppx	P Cycling	exopolyphosphatase	Inorganic P hydrolysis

pqq C	P Cycling	pyrroloquinoline-quinone synthase	Inorganic P solubilization
aps A	S Cycling	adenosine-5’-phosphosulfate reductase α subunit	S reduction
dsr A	S Cycling	sulfite reductase α subunit	S reduction
dsr B	S Cycling	sulfite reductase β subunit	S reduction
sox Y	S Cycling	sulfur-oxidizing protein	S oxidation
yed Z	S Cycling	sulfite oxidase	S oxidation

Table S3 The differential analysis of functional genes among different cropping patterns in Chifeng

Gene name	Rotaion vs Soybean	Corn vs Soybean	Corn vs Rotation
accA	ns.	*	ns.
aclB	ns.	*	***
acsA	*	*	***
acsB	ns.	***	***
acsE	*	ns.	**
amoA1	***	**	***
amoA2	ns.	**	*
amoB	*	**	***
amyA	ns.	***	***
apsA	*	**	***
apu	ns.	***	***
bpp	ns.	*	**
CDH	*	ns.	**
chiA	ns.	*	**
dsrA	*	ns.	***
dsrB	ns.	ns.	*
exoPG	ns.	ns.	ns.
frdA	ns.	ns.	ns.
gam	ns.	*	ns.
gcd	ns.	ns.	ns.
gdhA	*	**	***
glx	*	ns.	***
hao	***	*	***
IsoP	ns.	*	**
korA	**	*	***
lig	ns.	ns.	*
manA	*	**	***

mct	ns.	ns.	**
mmoX	*	ns.	**
mnp	**	***	***
mxaF	*	**	***
napA	ns.	ns.	ns.
nifH	**	ns.	***
nirK1	ns.	ns.	ns.
nirK2	ns.	*	*
nirS1	ns.	ns.	ns.
nirS2	ns.	*	*
nirS3	ns.	*	***
nosZ1	**	**	***
nosZ2	ns.	ns.	*
nxrA	ns.	*	ns.
pccA	ns.	ns.	ns.
pgg-mdh	***	*	***
phnK	ns.	ns.	***
phoD	ns.	***	***
pmoA	*	***	***
ppx	***	ns.	***
pqqC	ns.	ns.	ns.
rbcL	ns.	ns.	ns.
smtA	*	ns.	**
SoxY	***	**	***
UreC	ns.	ns.	ns.
xylA	**	ns.	***
YedZ	**	***	***

LSD *p* values, *ns.* represented $p > 0.05$, * $p < 0.05$,** $p < 0.01$,*** $p < 0.001$

Table S4 The differential analysis of functional genes among different cropping patterns in Heihe

Gene name	Rotaion vs Soybean	Corn vs Soybean	Corn vs Rotation
accA	*	ns.	*
aclB	0.06	ns.	0.069
acsA	0.054	ns.	0.068
acsB	ns.	ns.	ns.
acsE	ns.	ns.	ns.
amoA1	ns.	ns.	ns.
amoA2	ns.	ns.	ns.
amoB	ns.	ns.	ns.
amyA	ns.	ns.	ns.
apsA	ns.	ns.	ns.

apu	ns.	ns.	ns.
bpp	ns.	ns.	ns.
CDH	0.085	ns.	0.065
chiA	ns.	ns.	ns.
dsrA	**	ns.	*
dsrB	0.082	ns.	ns.
exoPG	ns.	ns.	ns.
frdA	0.079	ns.	*
gam	ns.	ns.	ns.
gcd	*	ns.	0.071
gdhA	0.078	ns.	ns.
glx	ns.	ns.	ns.
hao	ns.	*	*
IsoP	ns.	ns.	0.065
korA	ns.	ns.	ns.
lig	ns.	ns.	ns.
manA	ns.	ns.	ns.
mct	ns.	ns.	ns.
mmoX	ns.	ns.	ns.
mnp	ns.	ns.	ns.
mxaF	ns.	ns.	ns.
napA	ns.	ns.	ns.
nifH	ns.	*	ns.
nirK1	ns.	ns.	ns.
nirK2	ns.	ns.	ns.
nirS1	ns.	ns.	ns.
nirS2	ns.	ns.	ns.
nirS3	ns.	ns.	ns.
nosZ1	ns.	ns.	ns.
nosZ2	ns.	ns.	ns.
nxrA	ns.	0.057	ns.
pccA	ns.	ns.	ns.
pgg-mdh	ns.	*	0.075
phnK	ns.	ns.	ns.
phoD	ns.	ns.	ns.
pmoA	ns.	ns.	ns.
ppx	ns.	ns.	ns.
pqqC	ns.	ns.	0.08
rbcL	ns.	***	***
smtA	ns.	ns.	ns.
SoxY	ns.	ns.	ns.
UreC	ns.	ns.	ns.
xylA	ns.	ns.	ns.

YedZ	ns.	ns.	ns.

LSD *p* values, *ns.* represented $p > 0.05$, * $p < 0.05$,** $p < 0.01$,*** $p < 0.001$

Table S5 The permutational multivariate analysis of variance among deffrent cropping patterns

	comparison	CF	HH
Bacterial Community	Soyebean/Rotation	0.23**	0.53**
	Soybean/Corn	0.48**	0.68**
	Rotation/Corn	0.40**	0.26**
Fungal Community	Soyebean/Rotation	0.38**	0.61**
	Soybean/Corn	0.59**	0.71**
	Rotation/Corn	0.57**	0.37**
Bacteria-fungi Community	Soyebean/Rotation	0.34**	0.58**
	Soybean/Corn	0.57**	0.70**
	Rotation/Corn	0.53**	0.34**
Functional genes	Soyebean/Rotation	0.44**	0.30**
	Soybean/Corn	0.48**	0.14
	Rotation/Corn	0.78**	0.32*

p values are indicated by asterisks: *$p \leq 0.05$; **$p < 0.01$; ***$p < 0.001$.

Table S6 Spearman correlation between six ecological services and βNTI in different clusters

	Cluster 1	Cluster 2	Cluster 3	Cluster 4
Multifunctionality	-0.086	**0.519*****	-0.052	0.090
C degradation	-0.060	**0.515*****	-0.097	0.107
C fixation	-0.104	**0.514*****	-0.021	0.080
Methane metabolism	-0.096	**0.483*****	-0.009	0.040
N Cycle	-0.091	**0.555*****	-0.020	0.096
P Cycle	-0.068	**0.482*****	-0.012	0.021
S Cycle	-0.041	**0.429*****	-0.087	0.165

p values are indicated by asterisks: *$p \leq 0.05$; **$p < 0.01$; ***$p < 0.001$.

Table S7 Identified abundant functional microorganisms at the order level

Microorganisms group	Ecological functions	Reference

Micrococcales	Carbon cycle and potential in nitrogen cycle	(Argiroff et al., 2019; Guo et al., 2020; Liu et al., 2020; Wang et al., 2018)
Vicinamibacterales	Phosphate cycle	(Wu et al., 2022)
Burkholderiales	Phosphate and nitrogen cycle	(Estrada-De los Santos et al., 2001; Ishii et al., 2011; Ragot et al., 2015; Wang et al., 2018; Wu et al., 2022)
Rhizobiales	Nitrogen cycle and phosphate cycle	(Chen et al., 2021; Garrido-Oter et al., 2018; Peix et al., 2001; Wang et al., 2018)
Thermomicrobiales	Potential in phosphate cycle	(Wang et al., 2022)
Gemmatimonadales	Carbon cycle	(Fan et al., 2014; He et al., 2012)
Chitinophagales	Carbon cycle	(Carrion et al., 2019; Li et al., 2022)
Nitrospirales	Nitrogen cycle	(Xia et al., 2011)

Table S8 GeneBank ID of each complete genome downloading from GeneBank website

Taxonomy	ASV ID	GeneBank ID
Burkholderiales	1ed03691420c8fd886f8675239e73f12	CP002252
	f01f6795d9bd1f7e3549ff102ae12d06	CP000245
	f375a2f1dacc0966975cdcb744b2b59e	CP002877
	f375a2f1dacc0966975cdcb744b2b59e	CP002878
	fb882c744a00aaa972dc7b78fbe61e8b	CP053069
Micrococcales	091f0039f9699e2b582c467fb547c98d	CP013747
	894a9016f3aa1b852877cd7499355ee1	CP046121
	45b5b9bfcdfba8a94fca18a8035918b3	CP013979
	091f0039f9699e2b582c467fb547c98d	CP019304

Rhizobiales	26450c239ee044057fdb77c9ebcdf521	CP022998
	021a60490bbb93b30a1e1a0019223750	CP042331
	2fe1505db34e42a86d382eb7708a1be3	HE616890
	c4a8a6505f5fd0f838318f8a6d1b6a68	CP049258
	7d270de44de74aba09718adb015c6e3d	CP048834
Vicinamibacterales	383efdea14cf87d1d9b3cd3cb83089b5	CP015136

Table S9 Mantel tests of environmental variables against mean nearest taxon distance metric (βMNTD) of ecological clusters in agricultural soils

	Cluster 1	Cluster 2	Cluster 3	Cluster 4
pH	-0.006	0.680^{***}	0.815^{***}	0.695^{***}
DOC	-0.147	0.409^{***}	0.455^{***}	0.413^{***}
DON	0.209^{*}	0.467^{***}	0.374^{**}	0.436^{***}
NH_4^+	0.075	0.063	0.111	0.134^{*}
Fe^{2+}	0.106	0.722^{***}	0.720^{***}	0.724^{***}
Fe^{3+}	0.171^{**}	0.760^{***}	0.726^{***}	0.762^{***}
AFe	0.170^{***}	0.754^{***}	0.728^{***}	0.754^{***}
AP	0.139	0.545^{***}	0.415^{***}	0.480^{***}
TC	0.147^{*}	0.731^{***}	0.744^{***}	0.728^{***}
TN	0.169^{**}	0.720^{***}	0.747^{***}	0.749^{***}
C/N	-0.115	0.418^{**}	0.621^{***}	0.555^{***}
Herbicides residue	0.265^{***}	0.707^{***}	0.667^{***}	0.739^{***}
Sulfonylureas	-0.060	0.035	0.025	0.040
Amides	-0.204	0.147^{*}	0.168^{**}	0.154^{*}
Triazine	0.053	-0.001	0.027	0.028
Aryloxyphenoxypropionate	-0.147	-0.040	-0.021	0.029
Cyclic imine	0.163	-0.019	-0.051	-0.030
Heterocycles	0.374^{**}	0.552^{***}	0.488^{***}	0.542^{***}
Phenoxy acid	-0.007	-0.067	-0.025	-0.077
Substituted urea	-0.289	-0.019	0.010	0.003
Diphenyl ether	0.483^{***}	0.625^{***}	0.530^{***}	0.648^{***}
Imidazolinone	0.153	0.108	-0.003	0.044
Benzoylcyclohexanediones	0.353^{**}	0.419^{***}	0.079	0.241^{**}

p values are indicated by asterisks: $*p \leq 0.05$; $**p < 0.01$; $***p < 0.001$.

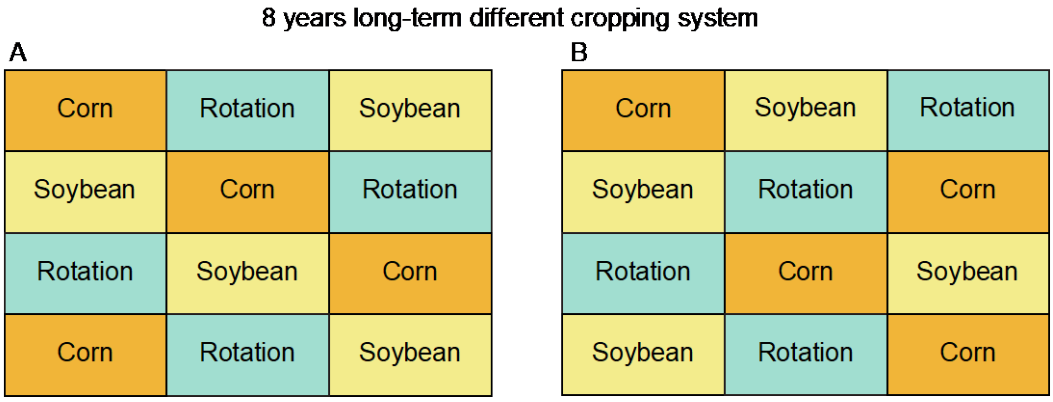

Fig. S1 Experimental design in different cropping systems in Chifeng (A) and Heihe (B). Soybean: continuous soybean cropping; Corn: continuous corn cropping; Rotation: soybean-corn rotation.

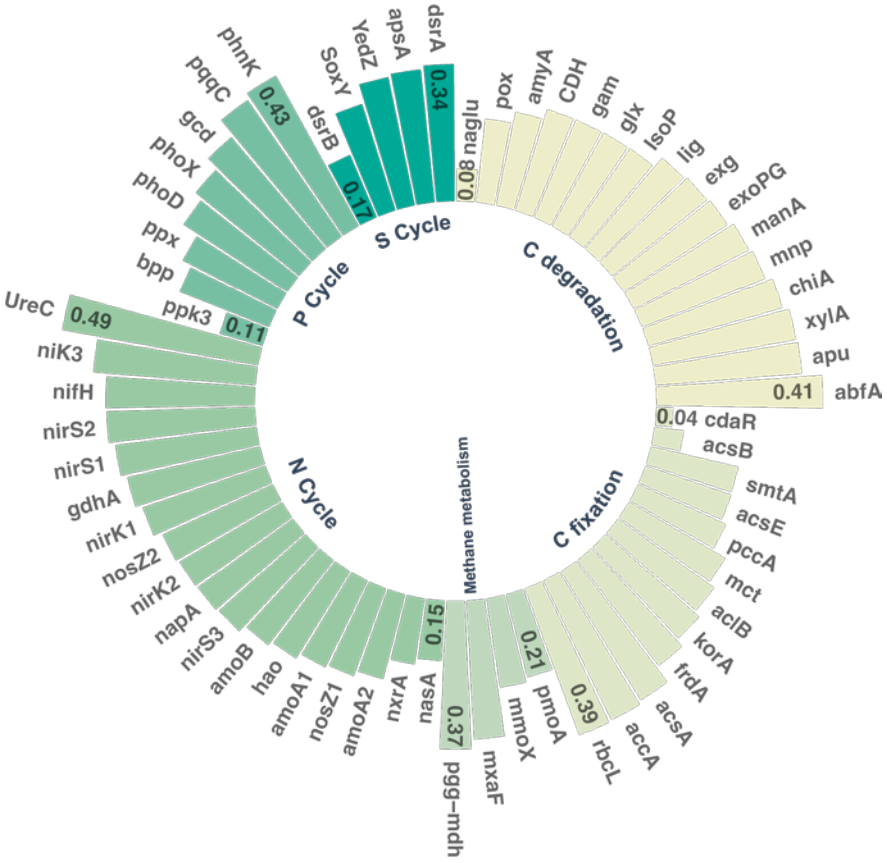

Fig. S2. The average abundance of functional genes in agricultural soils (max-min normalized).

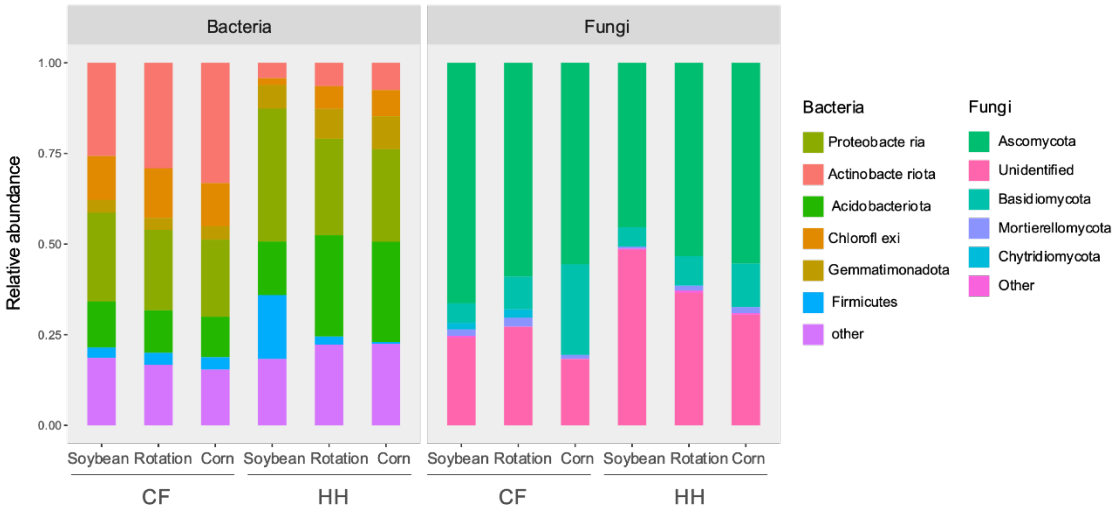

Fig. S3. Bacteria and fungi phylum composition among different cropping strategies.

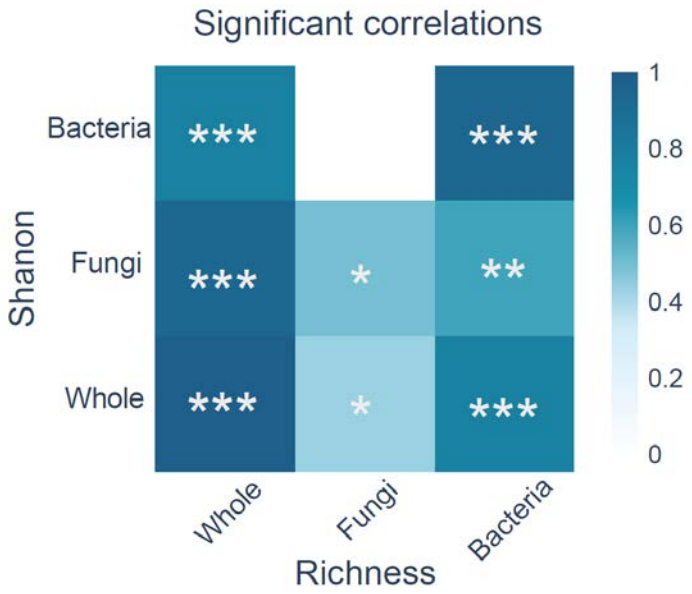

Fig. S4. Significant correlations (Spearman; *$p \leq 0.05$; **$p < 0.01$; ***$p < 0.001$) between Shannon index and richness (both indexes are min-max normalization) of selected groups of soil organisms.

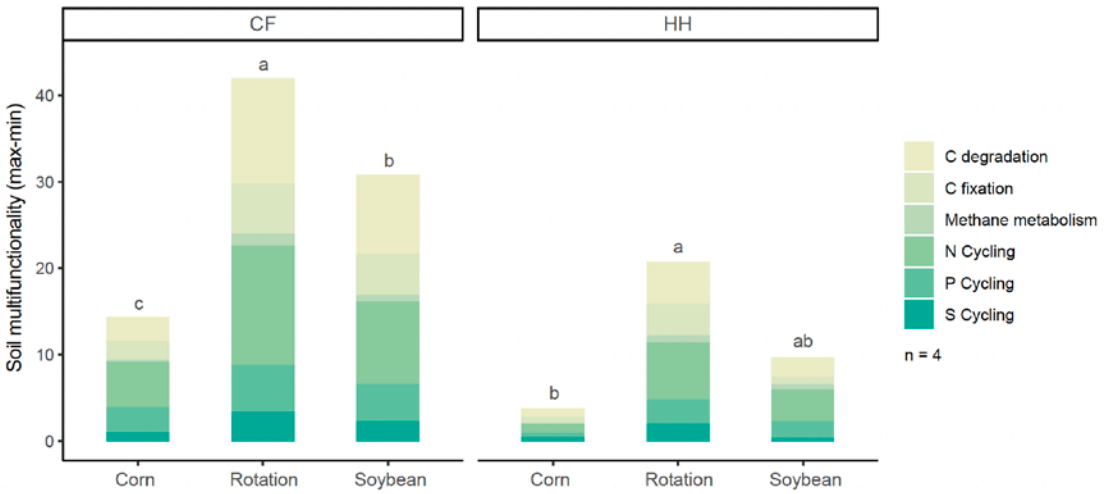

Fig. S5. Average multifunctionality index in response to cropping patterns. Different letters indicated significant differences (LSD). Abbreviations: CF, the Chifeng station; HH, the Heihe station.

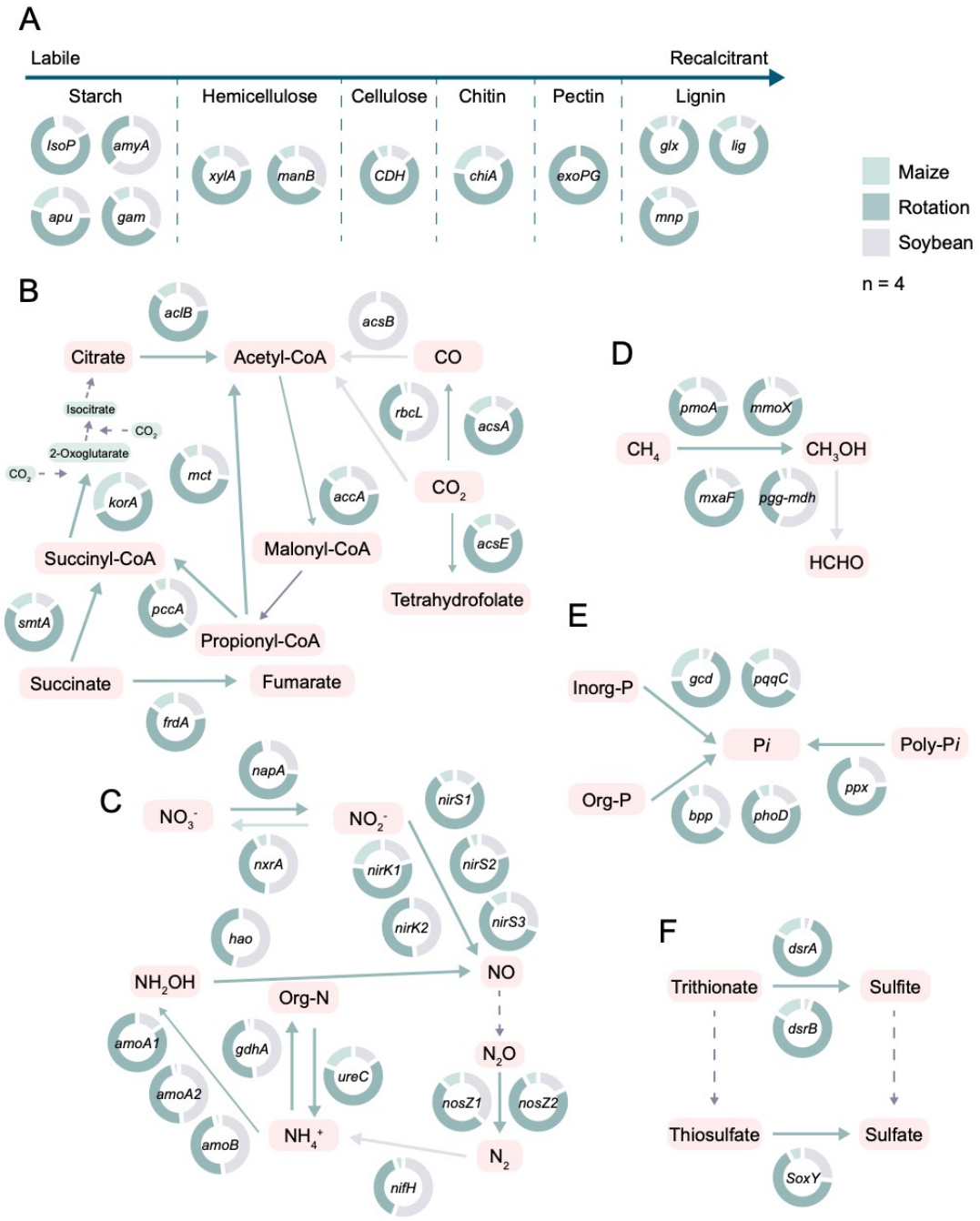

Fig. S6. The doughnut plot depicting the average abundance ratios of selected genes (max-min normalization) in Heihe station. Genes that have been selected exhibit a gene abundance percentage greater than 40% in at least one cropping system.The arrows of solid lines indicate that the genes involved in the metabolic pathway are quantified in this study, while the dotted arrows indicate that the metabolic pathway exists, but the genes involved are not

in this study. The color of the arrows in the solid line corresponds to a higher proportion of the gene in a cropping strategy than in the other, and the results of the analysis of variance were shown in Table S3. The metabolism pathway was exhibited according to KEGG (https://www.genome.jp/kegg/pathway.html).

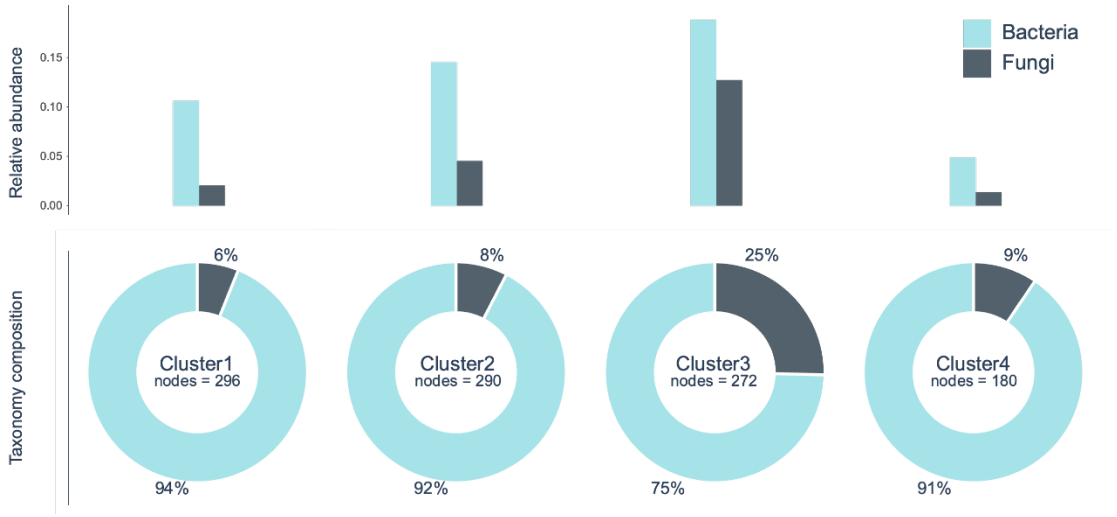

Fig. S7. The relative and proportion of bacteria and fungi among ecological clusters.

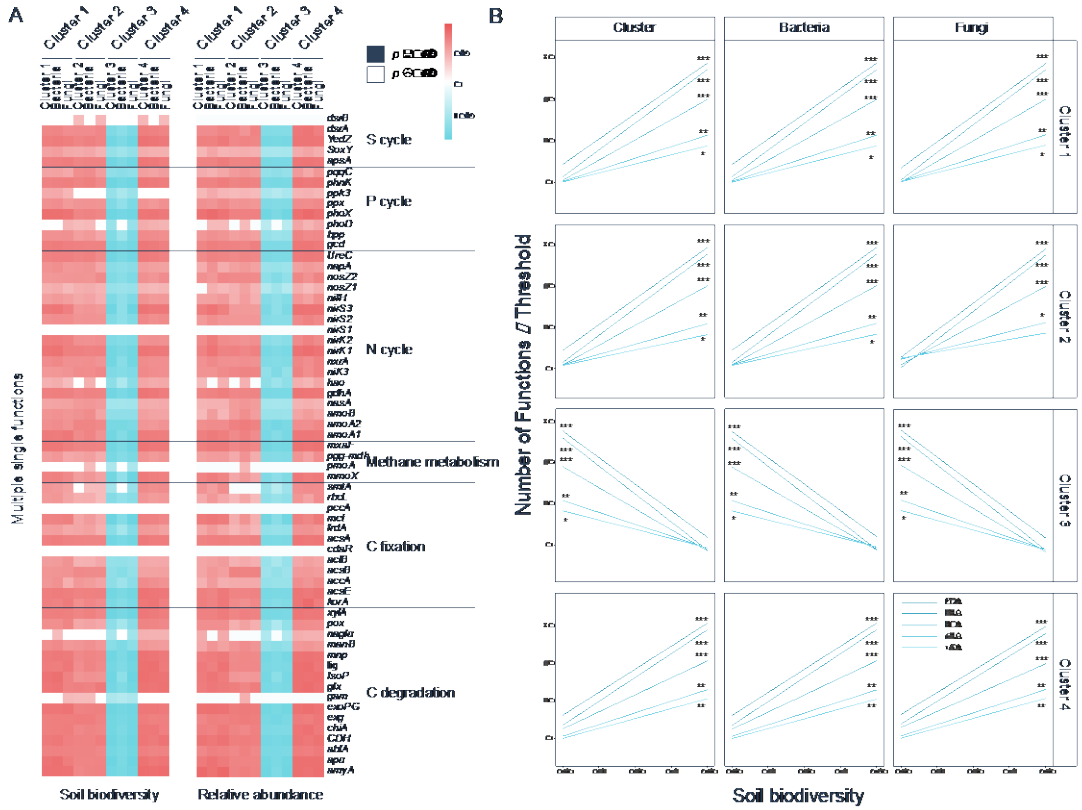

Fig. S8. Significant correlations (Spearman; $p \leq 0.05$) between the copies of functional genes and the biodiversity of ecological clusters or their abundance (A). The relationships between multithreshold functioning and the biodiversity of ecological clusters (min-max normalization richness of bacteria, fungi, and a composite metric of their joint diversity) (B); statistical analysis was performed using ordinary least squares linear regressions; p values are indicated by asterisks: *$p \leq 0.05$; **$p < 0.01$; ***$p < 0.001$.

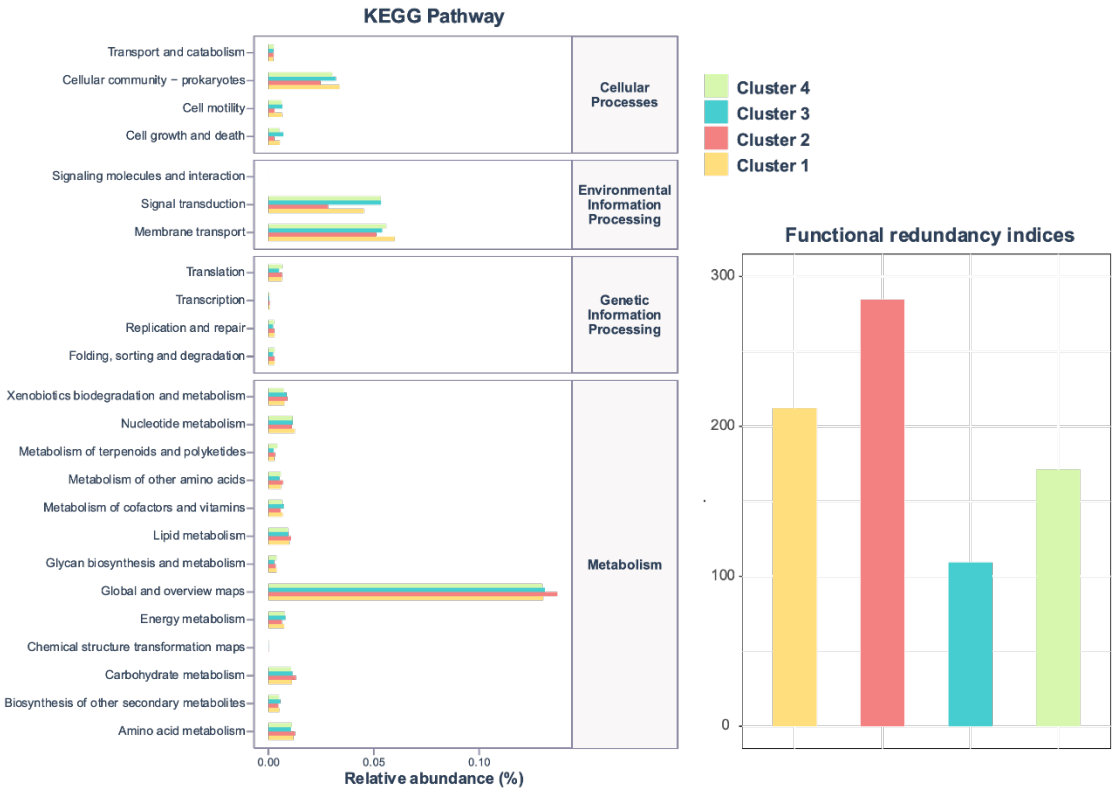

Fig. S9. The potential KEGG pathway of bacteria in clusters and functional redundancy indices were predicted based on their representative 16S rRNA gene sequences using R package *Tax4Fun2*.

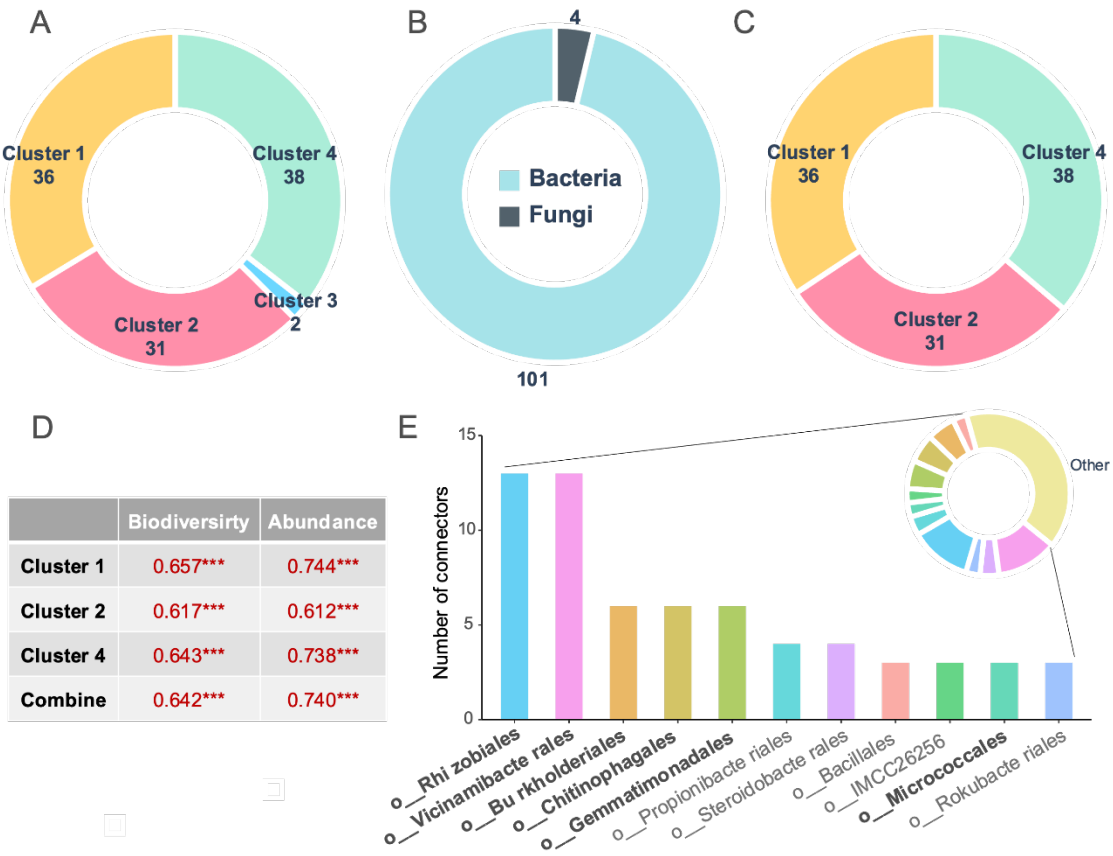

	Biodiversirty	Abundance
Cluster 1	0.657***	0.744***
Cluster 2	0.617***	0.612***
Cluster 4	0.643***	0.738***
Combine	0.642***	0.740***

Fig. S10. A, the number of identified connectors (*Pi* > 0.62) among individual clusters in the network; B, taxonomy composition of connectors in cluster 1, 2 and 4 at the kingdom level; C, after extracting keystone cluster 1, 2 and 4, the number of identified connectors (the *Pi* values were calculated all over again, and cut off in *Pi* > 0.62) among individual cluster; D, the relationships between biodiversity and relative abundance of connectors in individual cluster as well as combination of these connectors and the average multifunctionality. Statistical analysis was performed using ordinary least squares linear regressions; *p* values are indicated by asterisks: *$p \leq 0.05$; **$p < 0.01$; ***$p < 0.001$; E, bacterial taxonomy composition of connectors in cluster 1, 2 and 4 at the order level. Bold type annotations are presented the identified functional groups according to Table S4 (ordered by the number of connectors).

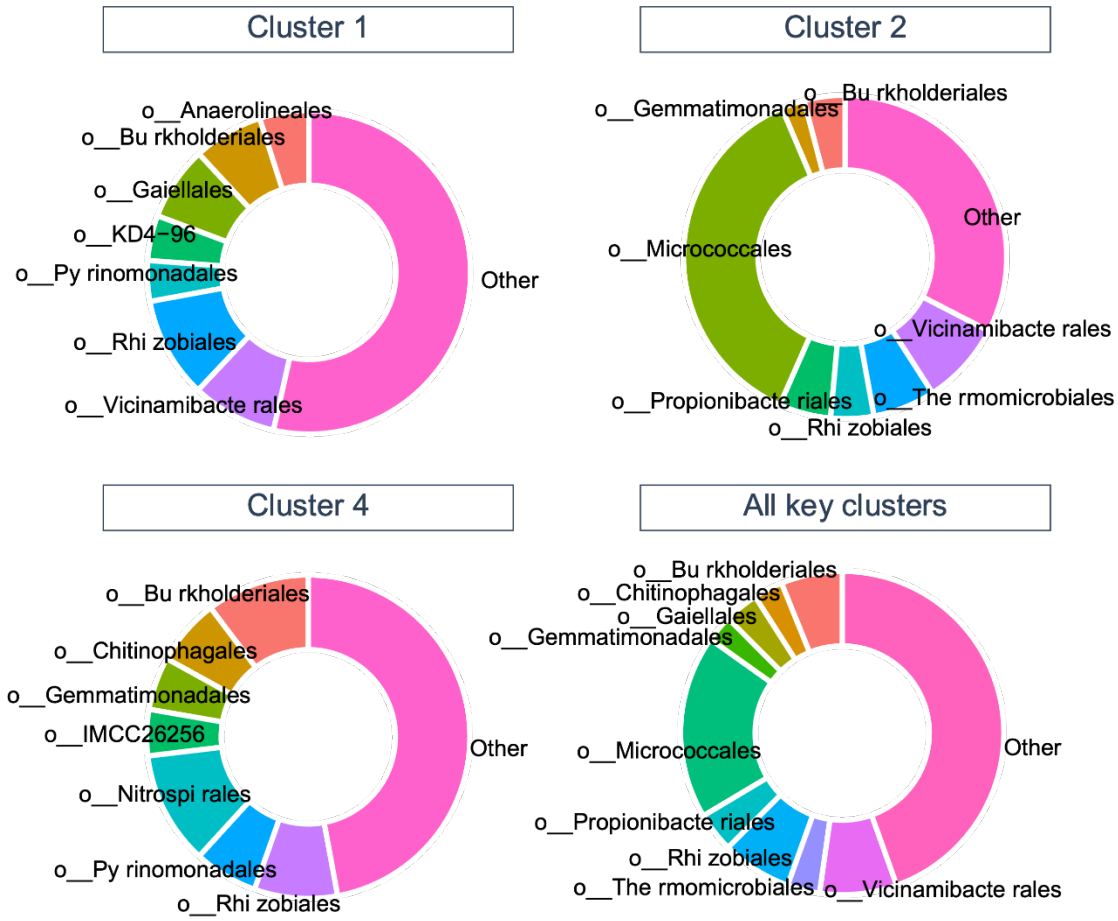

Fig. S11. The relative abundance of phylotypes at order level

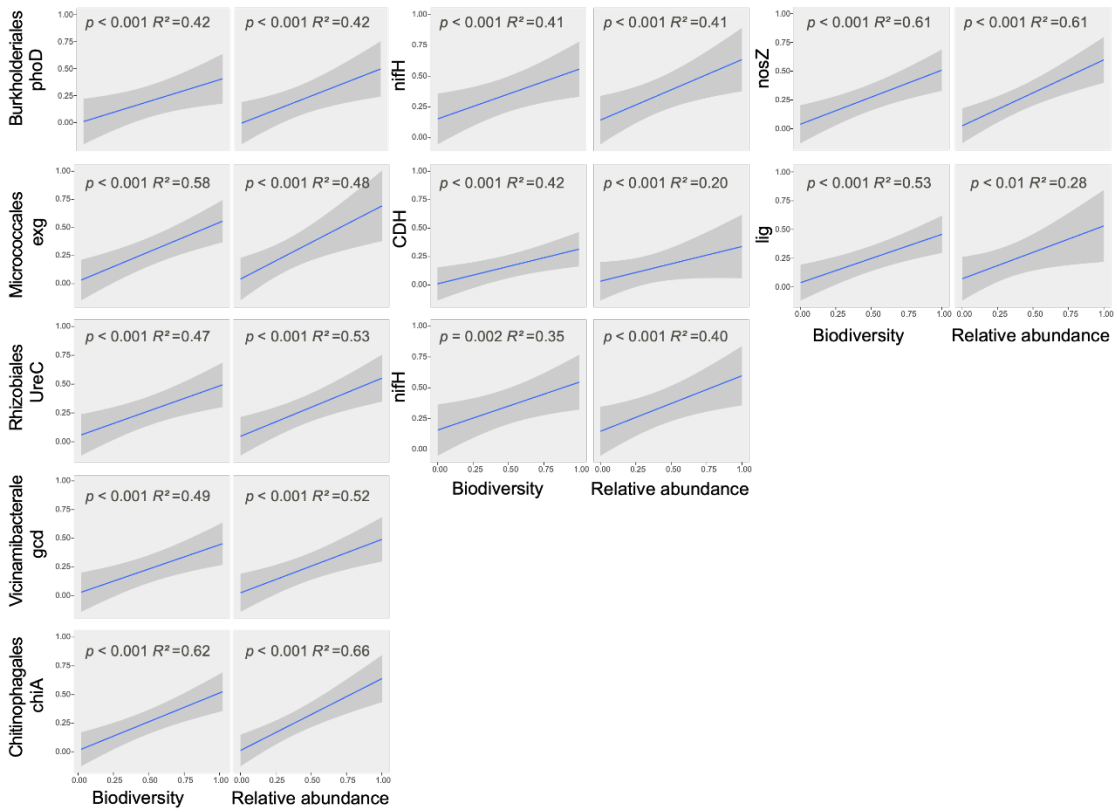

Fig. S12. The relationships between functional phylotypes in key-stone clusters and harbored genes referring to Table S4

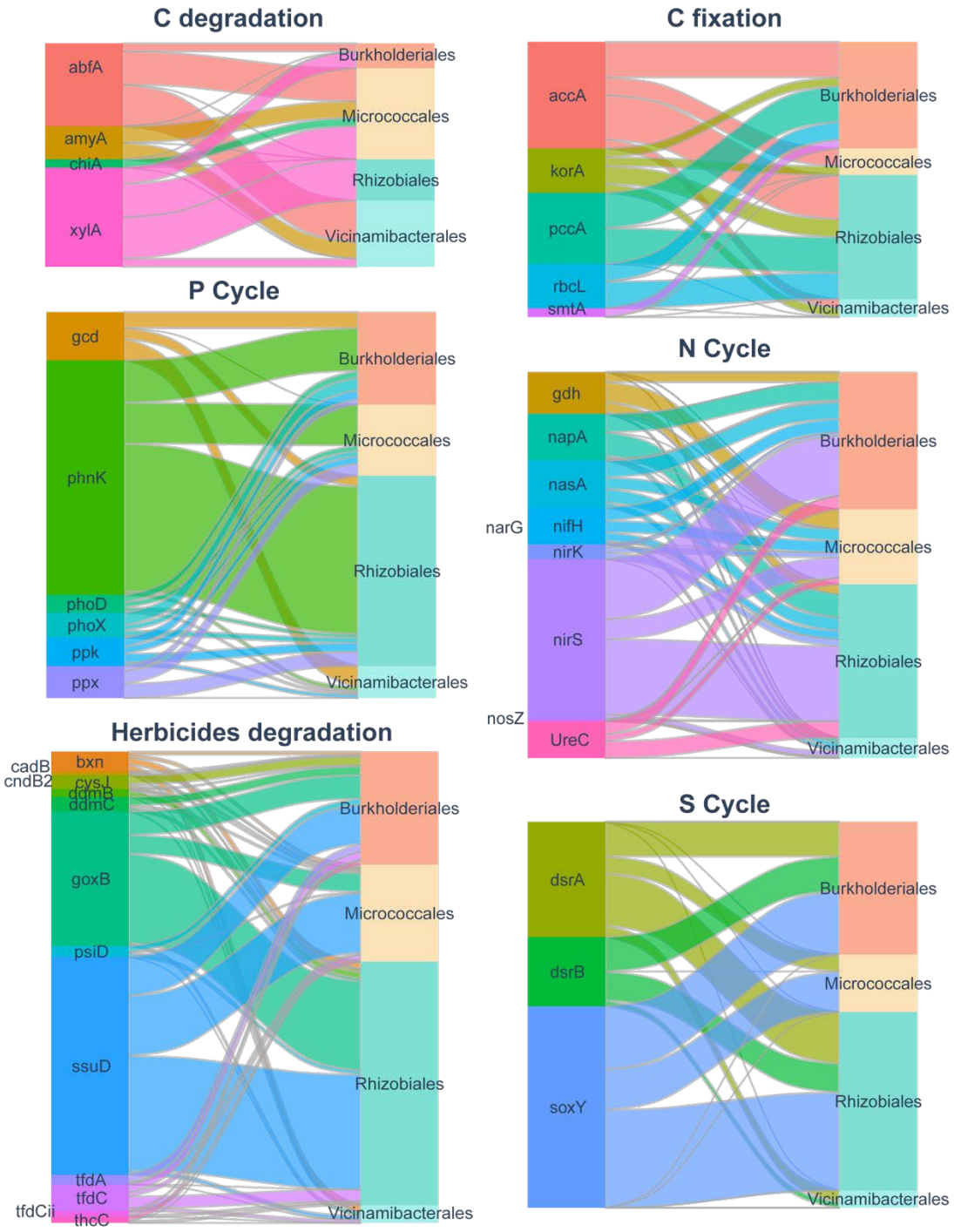

Fig. S13. Gene copies of dominant keystone phylotypes genome that were downloaded from GeneBank.

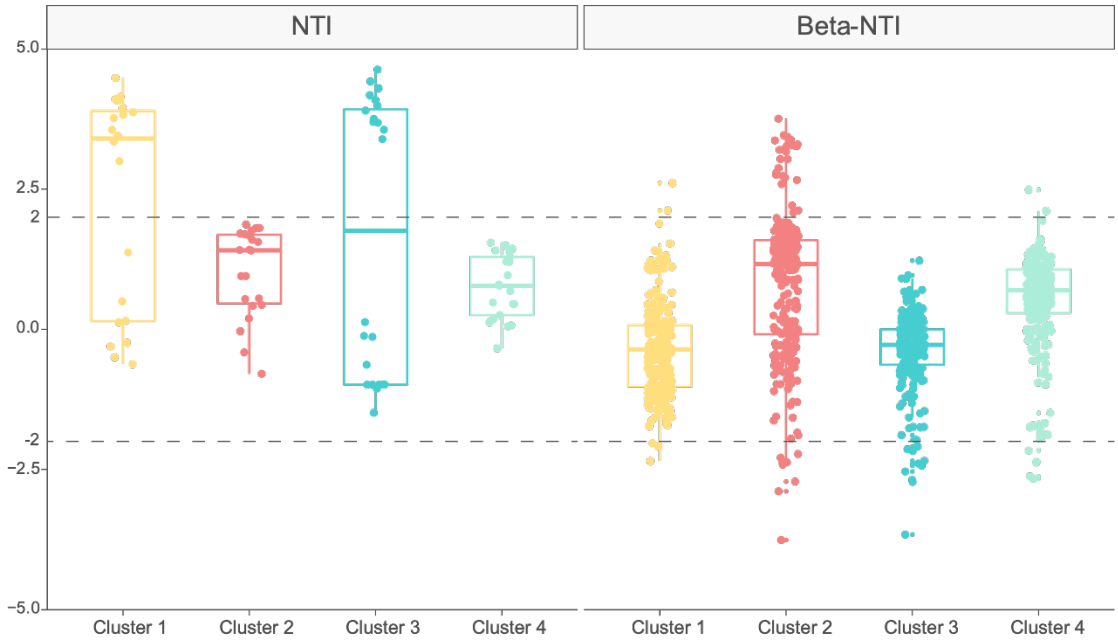

Fig. S14. The nearest taxon index (NTI) and β-nearest taxon index (βNTI) are among different ecological clusters.

Fig. S15. Significant correlations (Spearman; $p < 0.05$) between average multifunctionality and β-nearest taxon index (βNTI) (A). Relationships between βNTI of cluster 2 and differences in average multifunctionality and six soil ecological services for the abundant and rare subcommunities (B).

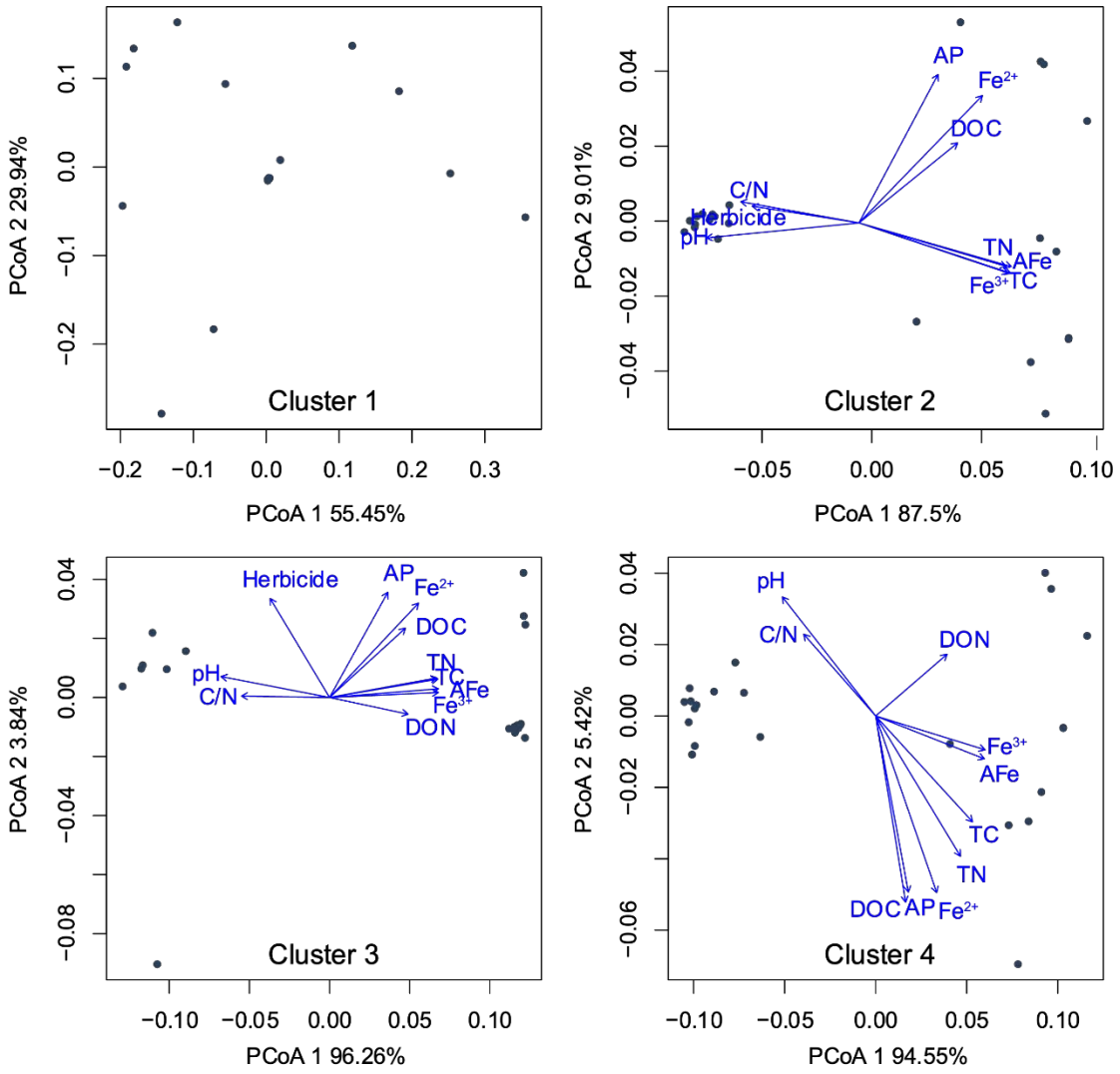

Fig. S16. Major environmental variables in shaping the ecological cluster phylogenetic sub-communities based on mean nearest taxon distance metric (βMNTD) identified by principal coordinates analysis (PCoA).

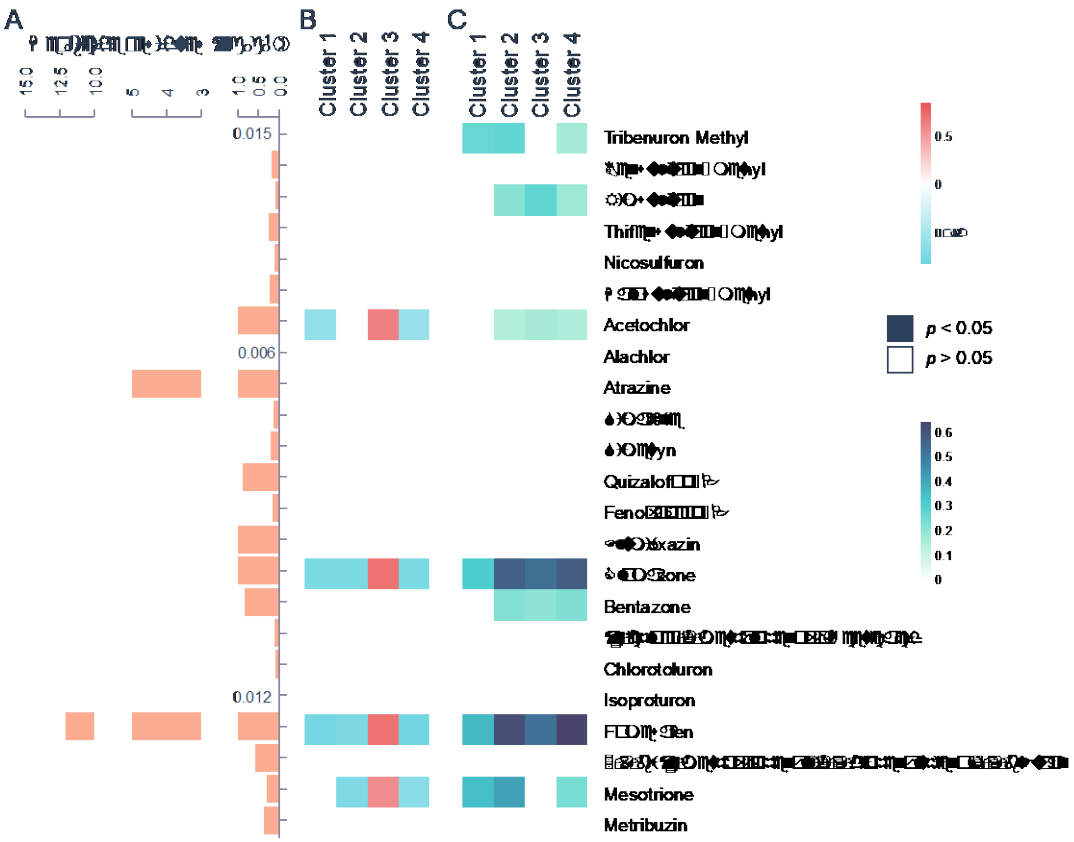

Fig. S17. The average herbicide residues in soil (A) and its significant association (Spearman correlation) with the biodiversity of identified cluster (B); the mean nearest taxon distance metric, being quantified by spearman correlation (C).

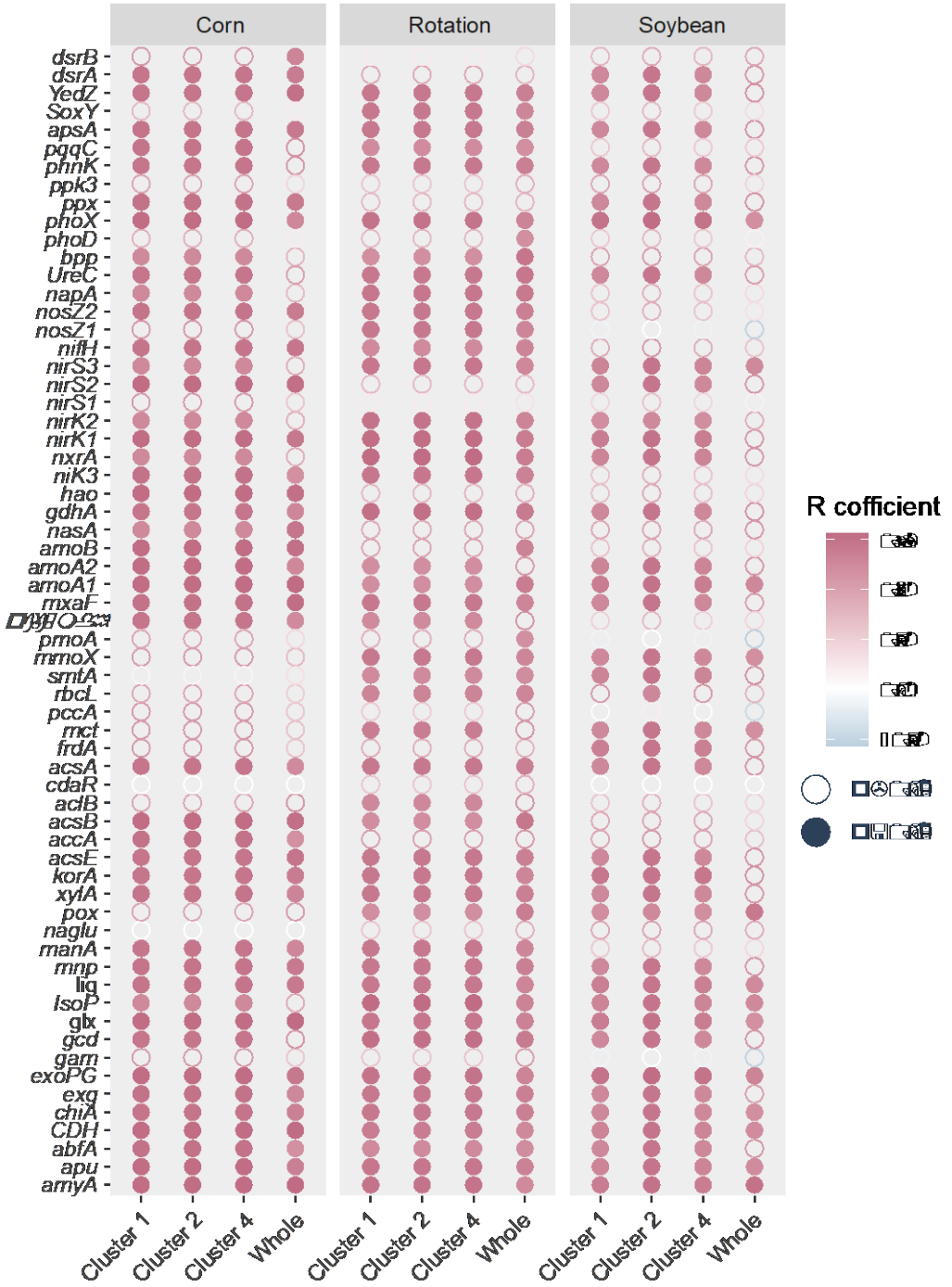

Fig. S18. Spearman correlations between the abundance of functional genes and biodiversity of keystone phylotypes (min-max normalized)

Reference

Argiroff WA, Zak DR, Upchurch RA, Salley SO, Grandy AS. Anthropogenic N deposition alters soil organic matter biochemistry and microbial communities on decaying fine roots. Global Change Biology 2019; 25: 4369-4382.

Buchfink B, Reuter K, Drost HG. Sensitive protein alignments at tree-of-life scale using DIAMOND. Nature Methods 2021; 18: 366-+.

Carrion VJ, Perez-Jaramillo J, Cordovez V, Tracanna V, de Hollander M, Ruiz-Buck D, et al. Pathogen-induced activation of disease-suppressive functions in the endophytic root microbiome. Science 2019; 366: 606-+.

Chen XD, Condron LM, Dunfield KE, Wakelin SA, Chen LJ. Impact of grassland afforestation with contrasting tree species on soil phosphorus fractions and alkaline phosphatase gene communities. Soil Biology & Biochemistry 2021; 159.

Cumbo F, Paci P, Santoni D, Di Paola L, Giuliani A. GIANT: A Cytoscape Plugin for Modular Networks. Plos One 2014; 9.

Delgado-Baquerizo M, Reich PB, Trivedi C, Eldridge DJ, Abades S, Alfaro FD, et al. Multiple elements of soil biodiversity drive ecosystem functions across biomes. Nature Ecology & Evolution 2020; 4: 210-220.

Estrada-De los Santos P, Bustillos-Cristales R, Caballero-Mellado J. Burkholderia, a genus rich in plant-associated nitrogen fixers with wide environmental and geographic distribution. Applied and Environmental Microbiology 2001; 67: 2790-2798.

Fan FL, Yin C, Tang YJ, Li ZJ, Song A, Wakelin SA, et al. Probing potential microbial coupling of carbon and nitrogen cycling during decomposition of maize residue by C-13-DNA-SIP. Soil Biology & Biochemistry 2014; 70: 12-21.

Fan KK, Delgado-Baquerizo M, Guo XS, Wang DZ, Zhu YG, Chu HY. Biodiversity of key-stone phylotypes determines crop production in a 4-decade fertilization experiment. Isme Journal 2020.

Feng JY, Xu Y, Ma B, Tang CX, Brookes PC, He Y, et al. Assembly of root-associated microbiomes of typical rice cultivars in response to lindane pollution. Environment International 2019; 131.

Fortmann-Roe S. Consistent and Clear Reporting of Results from Diverse Modeling Techniques: The A3 Method. Journal of Statistical Software 2015; 66: 1-23.

Garrido-Oter R, Nakano RT, Dombrowski N, Ma KW, McHardy AC, Schulze-Lefert P, et al. Modular Traits of the Rhizobiales Root Microbiota and Their Evolutionary Relationship with Symbiotic Rhizobia. Cell Host & Microbe 2018; 24: 155-+.

Guimera R, Amaral LAN. Functional cartography of complex metabolic networks. Nature 2005; 433: 895-900.

Guo TF, Zhang Q, Ai C, Liang GQ, He P, Lei QL, et al. Analysis of microbial utilization of rice straw in paddy soil using a DNA-SIP approach. Soil Science Society of America Journal 2020; 84: 99-114.

He R, Wooller MJ, Pohlman JW, Catranis C, Quensen J, Tiedje JM, et al. Identification of functionally active aerobic methanotrophs in sediments from an arctic lake using stable isotope probing. Environmental Microbiology 2012; 14: 1403-1419.

Huang YL, Dai ZM, Lin JH, Li DM, Ye HC, Dahlgren RA, et al. Labile carbon facilitated phosphorus solubilization as regulated by bacterial and fungal communities in Zea mays. Soil Biology & Biochemistry 2021; 163.

Huerta-Cepas J, Szklarczyk D, Heller D, Hernandez-Plaza A, Forslund SK, Cook H, et al. eggNOG 5.0: a hierarchical, functionally and phylogenetically annotated orthology resource based on 5090 organisms and 2502 viruses. Nucleic Acids Research 2019; 47: D309-D314.

Ishii S, Ohno H, Tsuboi M, Otsuka S, Senoo K. Identification and isolation of active N2O reducers in

rice paddy soil. Isme Journal 2011; 5: 1936-1945.

Jiao S, Lu YH, Wei GH. Soil multitrophic network complexity enhances the link between biodiversity and multifunctionality in agricultural systems. Global Change Biology 2022; 28: 140-153.

Li YZ, Li T, Wang ZT, Wang SN, Qin XL, Liao YC. Plastic film mulch changes the microbial community in maize root-associated compartments. Plant and Soil 2022; 470: 5-20.

Liu SL, Deng YQ, Jiang ZJ, Wu YC, Huang XP, Macreadie PI. Nutrient loading diminishes the dissolved organic carbon drawdown capacity of seagrass ecosystems. Science of the Total Environment 2020; 740.

Luo F, Zhong JX, Yang YF, Scheuermann RH, Zhou JZ. Application of random matrix theory to biological networks. Physics Letters A 2006; 357: 420-423.

Peix A, Rivas-Boyero AA, Mateos PF, Rodriguez-Barrueco C, Martinez-Molina E, Velazquez E. Growth promotion of chickpea and barley by a phosphate solubilizing strain of Mesorhizobium mediterraneum under growth chamber conditions. Soil Biology & Biochemistry 2001; 33: 103-110.

Ragot SA, Kertesz MA, Bunemann EK. phoD Alkaline Phosphatase Gene Diversity in Soil. Applied and Environmental Microbiology 2015; 81: 7281-7289.

Sun H, Wu Y, Zhou J, Yu D, Chen Y. Microorganisms drive stabilization and accumulation of organic phosphorus: An incubation experiment. Soil Biology and Biochemistry 2022; 172: 108750.

Tu QC, Lin L, Cheng L, Deng Y, He ZL. NCycDB: a curated integrative database for fast and accurate metagenomic profiling of nitrogen cycling genes. Bioinformatics 2019; 35: 1040-1048.

Wang JL, Liu KL, Zhao XQ, Gao GF, Wu YH, Shen RF. Microbial keystone taxa drive crop productivity through shifting aboveground-belowground mineral element flows. Science of the Total Environment 2022; 811.

Wang L, Luo XS, Liao H, Chen W, Wei D, Cai P, et al. Ureolytic microbial community is modulated by fertilization regimes and particle-size fractions in a Black soil of Northeastern China. Soil Biology & Biochemistry 2018; 116: 171-178.

Wu X, Rensing C, Han D, Xiao K-Q, Dai Y, Tang Z, et al. Genome-Resolved Metagenomics Reveals Distinct Phosphorus Acquisition Strategies between Soil Microbiomes. mSystems 2022: e0110721.

Xia WW, Zhang CX, Zeng XW, Feng YZ, Weng JH, Lin XG, et al. Autotrophic growth of nitrifying community in an agricultural soil. Isme Journal 2011; 5: 1226-1236.

Xu Y, He Y, Zhang Q, Xu JM, Crowley D. Coupling between Pentachlorophenol Dechlorination and Soil Redox As Revealed by Stable Carbon Isotope, Microbial Community Structure, and Biogeochemical Data. Environmental Science & Technology 2015; 49: 5425-5433.

Yu XL, Zhou JY, Song W, Xu MZ, He Q, Peng YS, et al. SCycDB: A curated functional gene database for metagenomic profiling of sulphur cycling pathways. Molecular Ecology Resources 2021; 21: 924-940.

Zeng JX, Tu QC, Yu XL, Qian L, Wang C, Shu LF, et al. PCycDB: a comprehensive and accurate database for fast analysis of phosphorus cycling genes. Microbiome 2022; 10.

Zhao KK, Ma B, Xu Y, Stirling E, Xu JM. Light exposure mediates circadian rhythms of rhizosphere microbial communities. Isme Journal 2021; 15: 2655-2664.